Challenge Journal of Structural Mechanics

Research Article

Finite element analysis of pre-stressed steel arch beams

Erkan Polat [a,*], Barlas Özden Çaglayan [b]

[a] *Department of Earthquake Engineering, İstanbul Technical University, 34457 Istanbul, Turkey*
[b] *Department of Civil Engineering, İstanbul Technical University, 34457 Istanbul, Turkey*

ABSTRACT

Techniques are being developed day-by-day to make it possible to pass through larger openings using smaller beam-column sections. Parallel to this trend, there is another necessity to produce not only smaller but also more economical and architecturally attractive beams. The aim of this study is to explain the structural behavior of steel arch beams reinforced using post-tension cables. Due to the effect of these, the arch beam load carrying capacity increases and a smaller sized optimized section can be obtained with a better architectural view. Moreover, it also allows better mechanical and applicable solutions for buildings. For a better understanding of the behavior of the reinforced beam, a steel beam and a steel arch beam with post-tensioned cables were modeled and analyzed using the SAP2000 finite element analysis computer program and compared with each other. In addition, full-scale specimens were prepared for testing to determine the structural behavior and compare the results with those from the computer modeling, the outcome of which was very promising. The similarity between the results inferred that no extra engineering knowledge and effort are needed to design such beams. The predicted (and proved by the testing) beam bearing capacity was 35% higher than that of the unreinforced beam. With just three full-scale tests completed, it was evident that the ratio (35%) could be increased by adjusting the cable post-tension force on much smaller sized beams.

ARTICLE INFO

Article history:
Received 5 December 2017
Revised 21 February 2018
Accepted 25 May 2018

Keywords:
Steel arch beams
Pre-stressed cables
Finite element analysis
Buckling analysis
Real model testing

1. Introduction

In the literature, research has been published to produce sophisticated design solutions for engineering problems and/or assemblies. Furthermore, the findings in this study also offer a sophisticated assembly strategy for long span beams that allows small beam sizes. At the same time, curbing building costs as well as allowing for architectural considerations in terms of aesthetic appearance are targeted in this study.

Using different materials or members is a method of improvement, and in this sense, the aim of this study was to use steel beams post-tensioned by cables in the same assembly. The cables, which can only carry tension forces, were placed at the tension zone of the beam. In order to increase the effect of the cable pre-tension force on the beam, the lower flange of the latter is shaped like an arch and a cable was connected to the beam-ends. The selected cable radius was 28 mm and nearly 10 t of pre-tension force was applied to it. Thus, with the reverse moment generated by post-tensioning of the cable in the beam, the bearing capacity was increased in the first step.

Beam sizes and spans can be very different depending on the requirement, thus a comparison was made between the actual test model of the beam and the finite element model, and the beam dimensions given in Fig. 1 were found to be within the scope of the testing possibilities.

In this study, increasing the arch of the beam bending and buckling load capacity with finite element buckling analyses and real laboratory test results were proven.

* *Corresponding author*. Tel.: +90-216-5507079 ; E-mail address: e.polat.m@gmail.com (E. Polat)
ISSN: 2149-8024 / DOI: https://doi.org/10.20528/cjsmec.2018.03.003

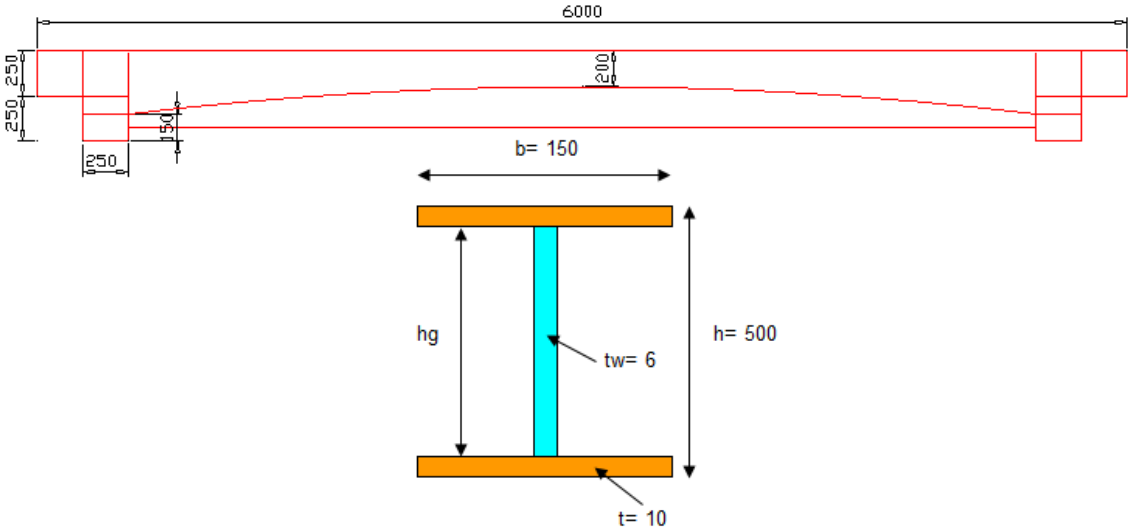

Fig. 1. Cross-section properties of the beam.

2. Section Properties

2.1. Materials

Steel beam flange and web plates : S235 JR
Cables : TS 1918 / 14 (AISI 316) (ϕ28 mm)
f_u = 180 kgf/mm²

2.2. Compactness

The section flange and web properties should provide compact section limits that prevent local buckling occurrences. Accordingly, the requirements for section properties were fulfilled by the section ratios selected, as can be seen in Eqs. (1a) and (1b) (AISC 360, 2010).

$$\frac{b}{2t} < \left(0.38\, x \sqrt{\frac{Es}{Fy}}\right) \quad , \quad 7.50 < 8.87 \surd \quad , \tag{1a}$$

$$\frac{hg}{tw} < \left(3.76\, x \sqrt{\frac{Es}{Fy}}\right) \quad , \quad 80 < 111.2 \surd \quad . \tag{1b}$$

2.3. Compression flange safety stress

Because of the variable section shape of the beam, compression safety stress changed along with section height. Maximum stress occurred at the mid-section of the span, thus the safety stress of the beam was calculated based on this location according to IMO - 02/2008 (2008) as follows:

$$\sigma_{B,\gamma} = \frac{2}{3}\left[1.0 - \frac{\sigma_a}{6B\sqrt{{\sigma_{s\gamma}}^2 + {\sigma_{w\gamma}}^2}}\right]\sigma_a \le 0.6\sigma_a \ , \tag{2a}$$

$$\sigma_{B,\gamma} = B\sqrt{{\sigma_{s\gamma}}^2 + {\sigma_{w\gamma}}^2} \ , \tag{2b}$$

$$\sigma_{B,\gamma} = \sigma_a/3 \ , \tag{2c}$$

$$\sigma_{Bs\gamma} = \frac{8440}{h_s l d_0/A_b} \ . \tag{2d}$$

l : 600 cm
d_o : 20 cm
b : 15 cm
d_i : 50 cm
t_f : 1 cm
t_w : 0.6 cm
γ : 1,5 < 8,043

$$h_s = 1.0 + 0.0230\gamma\sqrt{ld_o/A_0} \ , \tag{2e}$$

$$h_w = 1.0 + 0.00385\gamma\sqrt{l/i_{\gamma 0}} \ . \tag{2f}$$

A_{ko} : 40.8 cm²
A_{bo} : 58.8 cm²
r_{ky} : 3.31
r_{by} : 3.1
h_s : 1.59
h_w : 1.08
σ_s : 1.803 t/cm²
σw : 0.314 t/cm²

$$\sigma_s = \frac{8440}{h_s l d_0/A_b} \ , \tag{2g}$$

$$\sigma_{w\gamma} = \frac{120000}{(h_w l/i_{\gamma 0})^2} \ , \tag{2h}$$

$$B = 1.0 + 0.37\left[1.0 + \frac{M_1}{M_2}\right] + 0.50\gamma\left[1.0 + \frac{M_1}{M_2}\right] \ge 1.0 \ . \tag{2i}$$

M_1 : 0 t.cm
M_2 : 914 t.cm
x : 0.55
y : 2.2
B : 4.85 > 1
σ_b : 1.528 t/cm2 > 0.80 t/cm2
1.528 t/cm2 < 1.44 t/cm2
σ_b : 1.44 t/cm²

3. Finite Element Modeling

3.1. Loads

The loads applied to the beam were chosen so that the safety stress remained within its limits as given by the codes. It was assumed that loads were distributed uniformly and were applied on the top flange of the beam. This distributed load was calculated by considering a beam spacing of 1 m as follows:

Live Load	: 1300 kg/m^2
15 cm Concrete Slab	: 375 kg/m^2
10 cm Screed Concrete	: 240 kg/m^2
Cover	: 70 kg/m^2
Total Dead Load	: 685 kg/m^2

3.2. Design

The arch beam was modeled using the SAP2000 finite element analysis software package with shell members. A pre-tensioning steel cable was also attached to the beam-ends (see Fig. 2). The top flanges of the beam were not fixed along the span against lateral buckling.

4. Analysis Results

4.1. Shell stress and displacement

The tension force obtained on the upper flange of the beam was slightly greater than the limit tension force given in code (IMO - 02/2008, 2008), as can be seen in Figs. 3 and 4. The displacement/deflection occurred in a negative direction with a value of -12.6 mm.

Additionally, the cable tension force raised up from 10 to 18.6 t where the carrying capacity of the cable safety load was 50 t.

-12.65 mm displacement was obtained on the mid of the beam under the dead and live loads with pretension. L/300 = 6000/300 = 20 mm > 12.65 mm.

The analysis of the pre-tensioned arch beam tested in this study was compared to the results obtained from a conventional (hot-rolled) beam having a constant section height of 500 mm, as can be seen in Fig. 5. It was assumed that the span length under the same applied loads was the same. It can be observed that the proposed arch beam bearing capacity could be increased 1.45 times compared to the conventional beam design based on the allowable stress design (AISC 360, 2010).

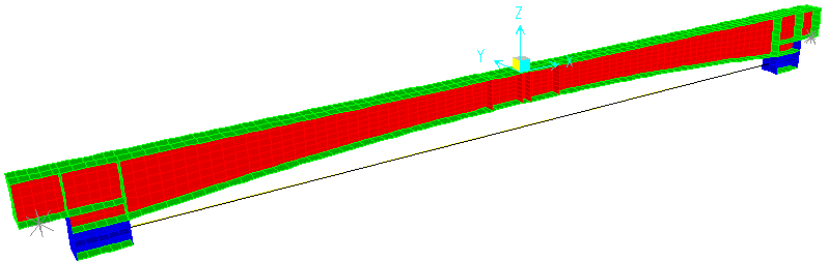

Fig. 2. Finite element model of the arch beam.

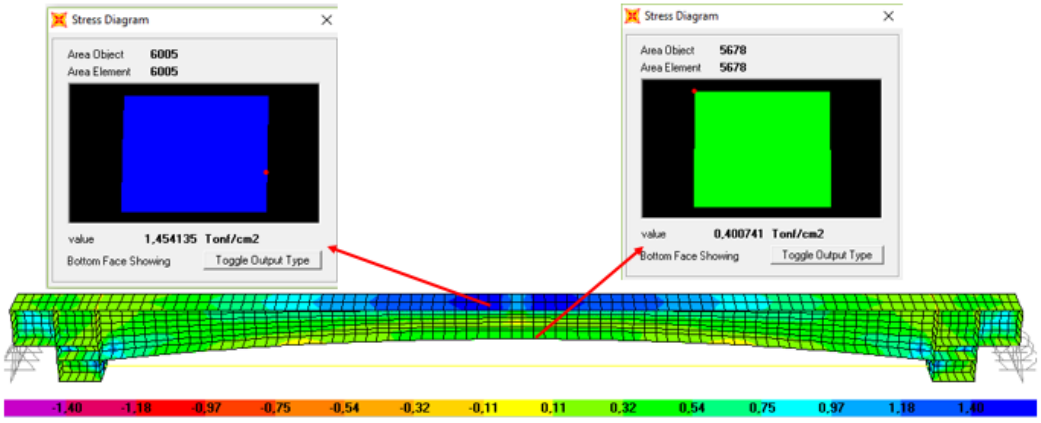

Fig. 3. Beam stress diagram (t/cm^2).

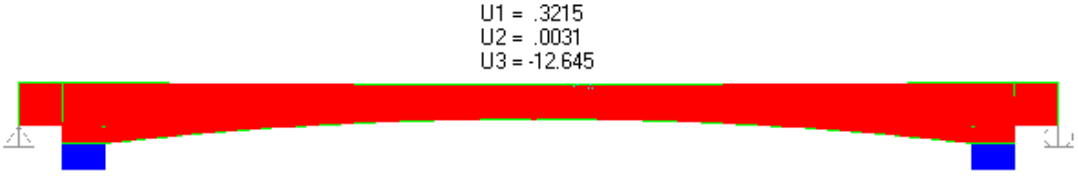

Fig. 4. Beam displacement dead + live load (mm).

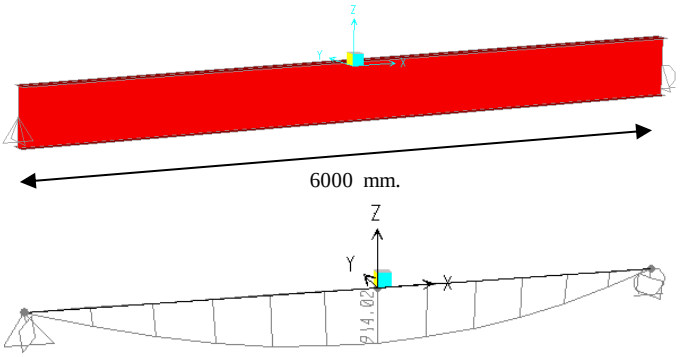

Fig. 5. Conventional I beam and moment diagram.

M 33 : 913.93 t.cm.
Mn / Ω : 629 t.cm (Beam moment capacity)

Beam capacity ratio : M33/(Mn/Ω) = 913/629 = 1.45 (AISC 360, 2010)

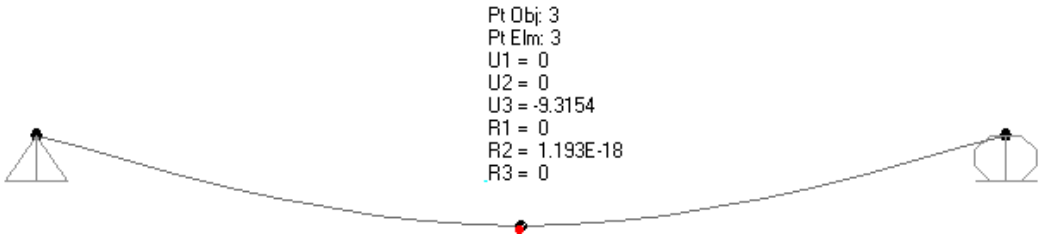

δ= 9.32 mm < 20 mm
Displacement values in directions; U1: X, U2: Y, U3: Z.

Fig. 6. Conventional I beam maximum vertical displacement.

The beam maximum vertical displacement (9.32 mm) was less than the arch beam displacement (20 mm), which is a disadvantage for arch beams under live loads, but the pre-tension is an advantage for dead and super dead loads because of the negative displacement.

4.2. Buckling analysis comparison

The conventional I beam and pre-tensioned arch beam buckling analysis results were compared with each other under the same given load.

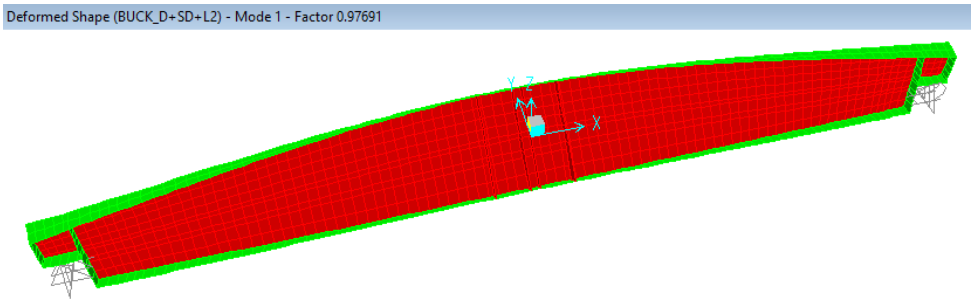

Fig. 7. Conventional I beam buckling analysis results.

Here, to obtain the same support conditions for a conventional beam modified as an arch beam, the conventional I beam first mode buckling factor was 0.977. This was not enough to be a safety concern since it is recommended that it is more than 2.

The first buckling factor of the arch beam was 2.765 in spite of the beam section size being reduced compared to the conventional I beam, which demonstrates a very important advantage of slender section beams. In this case, it was proved that the safety factor of the beam buckling was increased by the arch section and the pre-tension.

5. Specimen Tests

Three test specimens were produced according to the finite-element-analysis model-beam sizes and placed in the laboratory (see Fig. 9). The main loading frame consisted of HEA 300 profiles. These frames were analyzed under the maximum test load and capacity of the beam being tested.

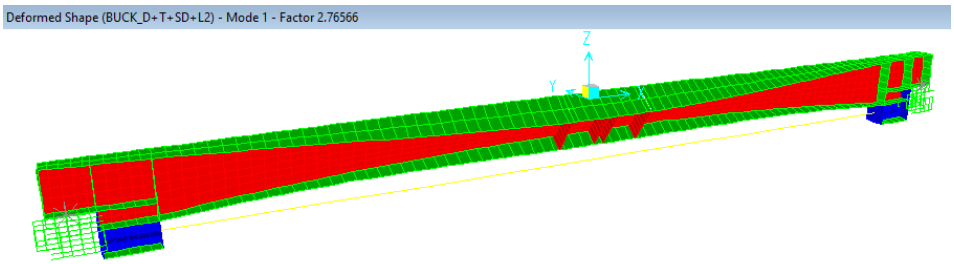

Fig. 8. Pre-stressed arch beam buckling analysis results.

Fig. 9. Test specimen.

One vertical and 3 horizontal displacement meters (linear variable differential transformers) were used. A total of 18 strain gauges were used on the test beam to measure the stresses and the tension in the rope. Two accelerometers were placed on the beams to monitor horizontal and vertical vibrations and another one was placed on the cable.

The first two samples were tested by increasing the applied loads up to the beam flange reach the yield limit. And second time, same two samples were forced to the ultimate state so that their bearing capacities were obtained, and the remaining one sample was loaded without a cable. Finally, total 5 tests were completed.

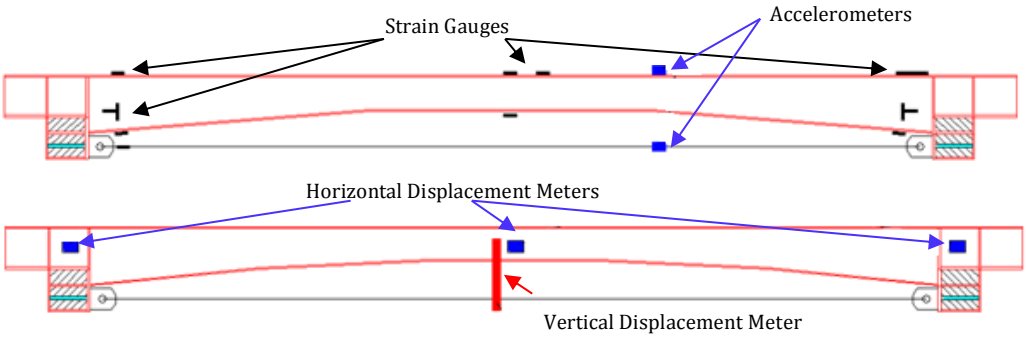

Fig. 10. Locations of the displacement meters, strain gauges, and accelerometers.

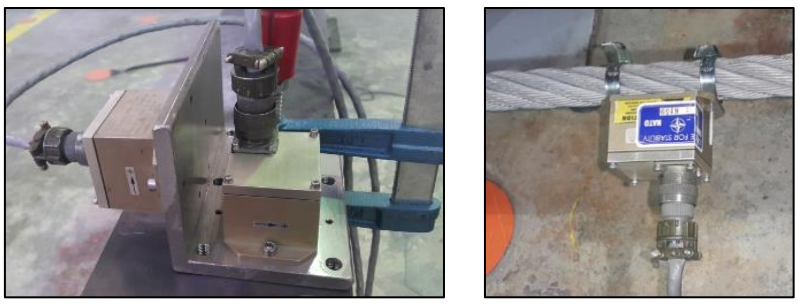

Horizontal & Vertical Accelerometer Cable Accelerometer

Fig. 11. Accelerometers.

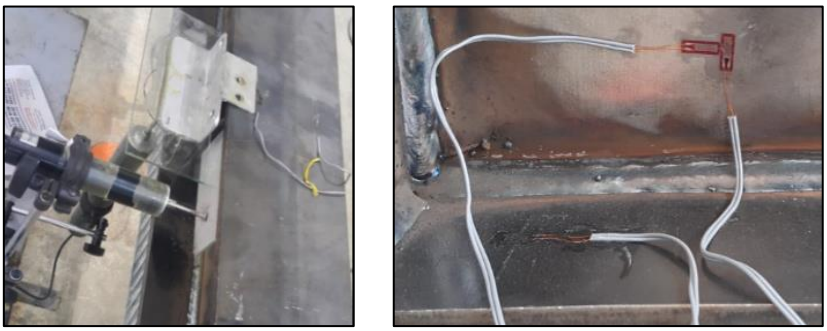

Fig. 12. Displacement transducers and strain gauges.

To measure the cable force, the results from the accelerometer and strain gauges were evaluated together. For this, the formulas reported by Wang et al. (2000):

$$T = 4ml^2 \frac{f_n^2}{n^2}, \tag{3}$$

and Humar (1990):

$$T = 4ml^2 \frac{f_n^2}{n^2} - \frac{EI}{\beta}(n\pi)^2, \tag{4}$$

were used and the values compared with the test results obtained from the strain gauges. However, according to the formulas, they were quite different from the strain gauge results.

Finally, the recordings of the accelerometers on the cable were transformed using the formulation developed by Fang and Wang (2012), and it can be seen that the results were subsequently very close.

In Fig. 13, the computer model and the results obtained from the test (test number 4) were demonstrated comparatively by applying a vertical concentrated load of 10 t. The test results were arranged in the Excel program and show the relevant parts of the beam image.

The strain distribution in the pre-tensioned arch bridge proposed in this study according to the test results recorded from the strain gauges is shown in Fig. 15.

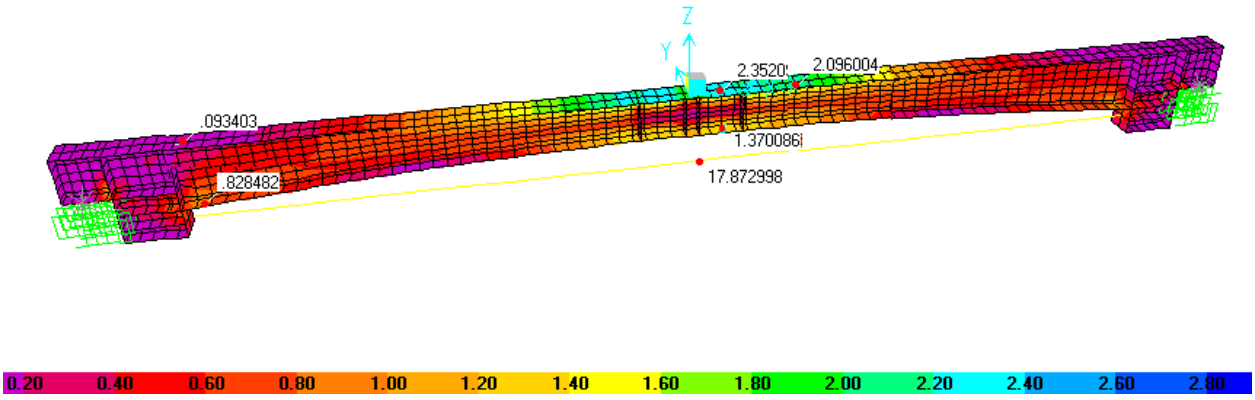

Fig. 13. Beam stress distribution (t/cm²).

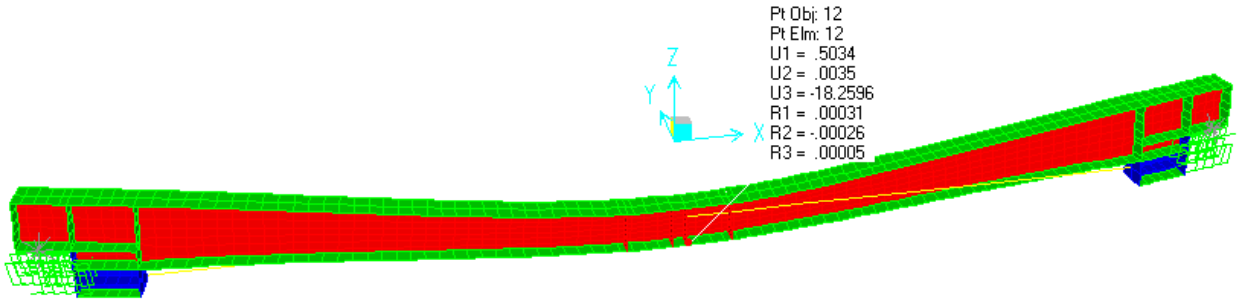

Displacement values in directions; U1: X, U2: Y, U3: Z.
Rotations around the related axis; R1, R2, and R3.

Fig. 14. Beam displacements (mm).

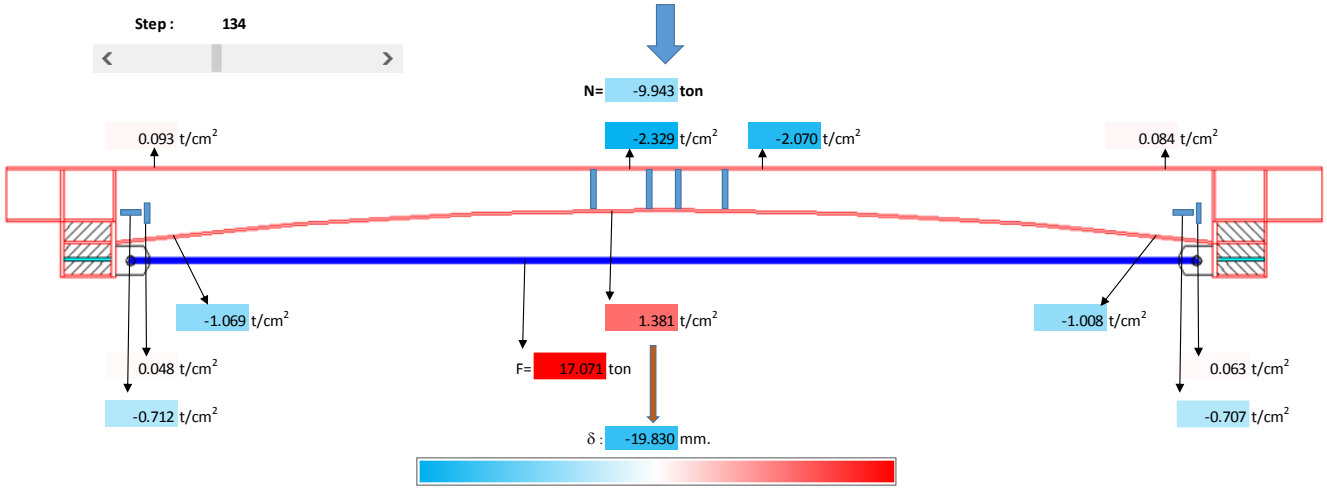

Fig. 15. Beam stress and displacement test results.

As can be seen, the stresses (at the mid-point 2.32 ≅ 2.35 t/cm²), displacement (19.83 ≅ 18.26 mm), and cable forces (17.07 ≅ 17.87 t) were reasonably close to each other.

The results obtained from the accelerometers were subjected to a fast Fourier transform (FFT) so that the cable forces could be calculated in terms of frequency (Fig. 16).

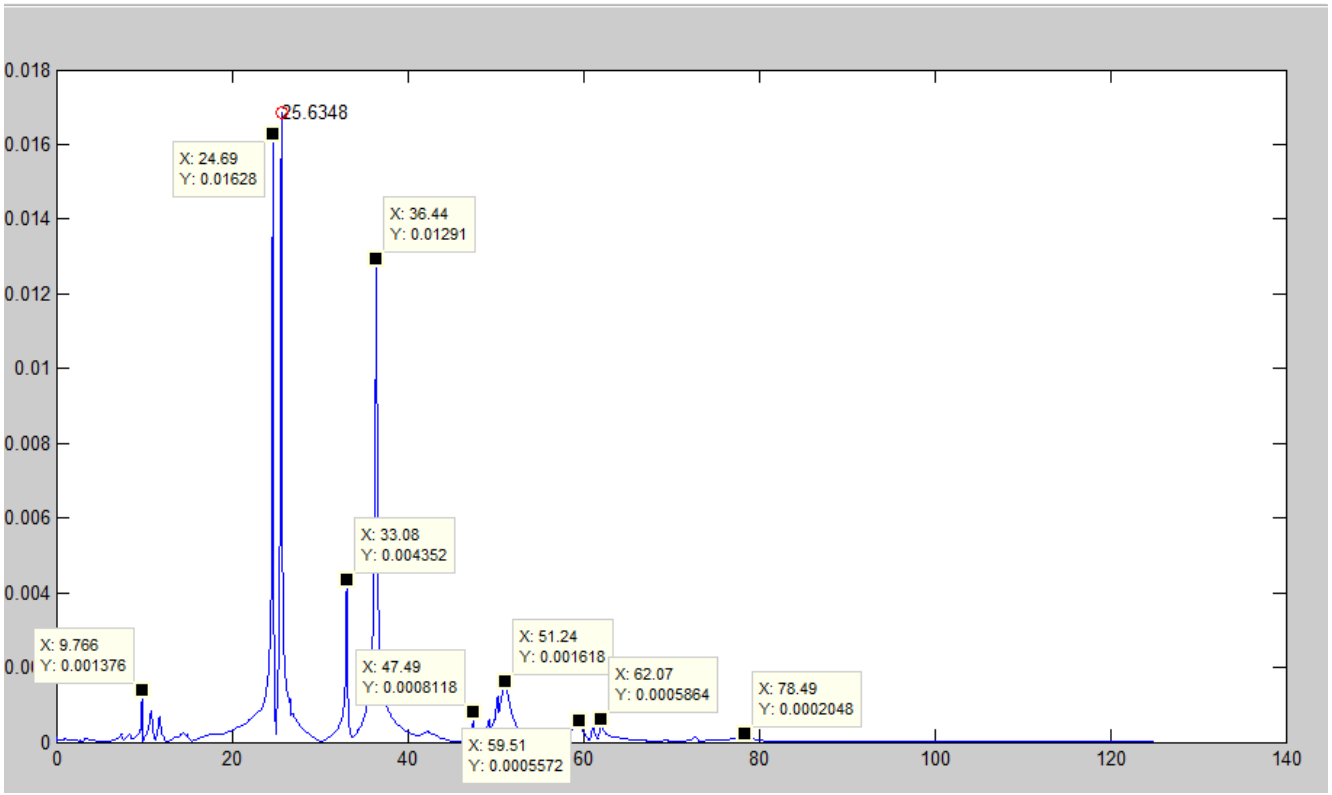

Fig. 16. Cable accelerometer FFT results for Test 4. Cable force = 16.9 t.

At 26.63 Hz, nearly all of the FFT results could be observed, so it was understood that this was the frequency of the systems and was consequently ignored. When all of the FFT results were compared, it is noticeable that between 27.16 Hz (Cable force 10.17 t) and 39.95 Hz (Cable Force 23 t), the frequencies changed due to the cable forces. Therefore, it is understood that the cable frequency was 36.44 Hz (Cable Force 16.9 t). Table 1 contains a detailed comparison in which all of the close FFT frequencies are presented one under the other; variable frequencies were chosen according to cable forces.

Vertical and horizontal accelerometer results were at the same frequencies as the cables.

$$T = 4\pi^2 ml^2 \frac{f_n^2}{\gamma_n^2} - \frac{EI}{l^2}\gamma_n^2 , \tag{5a}$$

$$\gamma_n^2 = n\pi + A\psi_n + B\psi_n^2 , \tag{5b}$$

$$A = -18.9 + 26.2n + 15.1n^2\ ,\ B = \begin{cases} 290 & (n = 1) \\ 0 & (n \geq 2) \end{cases}\ , \quad (5c)$$

$$\psi_n = \sqrt{\frac{EI}{m\omega_n^2 l^4}}, \quad (5d)$$

where;
T : Cable tension force
n : Mode number
ω_n : Angular frequency
E : Elastic modulus
m : Mass
l : Cable length
I : Moment of inertia

Table 1. Comparison of FFT results.

TEST -4 Force (t)		Frequency							1.Mod					2.Mod	
10.17	Cable		8.42	18.2	22.09	25.65			27.16	38.38	42.88	50	53.16	64	
	Horizontal					25						50			
	Vertical		8.42	19.56	22.09	25.7				38.36					
11.07	Cable		8.04	15.87	22.51	25	26.9		28.12		44.31	49.97		65.14	
	Horizontal					25							50		
	Vertical		8.04	15.87	22.5		26.93			39.9					
12	Cable	5.53	8.2	16.2	23.28	25	27.72		28.9	37.98	41.28		51.3	68.9	
	Horizontal	5.55	8.2	16.2					28.3				51.16		
	Vertical		8.2	16.2	23.27		27.74		28.3		41.28			63.37	
12.9	Cable		8.71	16.48	24.08		28.78		29.88		42.6		52.43		70.47
	Horizontal		8.71	16.48			28.79						52.51		
	Vertical		8.71	16.46	24.09		29.17				42.6			66.57	
14.1	Cable		9.95		24.92		28.72		32.98		44.22		57.31		72.79
	Horizontal		9.95				28.67		32.99		46.88				
	Vertical		9.95		24.92				32.99		44.22		57.13	66.6	
15	Cable		9.95			25.67	29.14		33.2		45.4				74.64
	Horizontal		9.95				29.31		33.23		48.39				
	Vertical					25.67	29.15		33.23		45.39				
15.9	Cable		9.74	15.56	24.1	25.36	26.18		34.12		46.46	49.58	58.94		76.1
	Horizontal		9.76		24.12	25.35		32.93	33.77		49.55		54.02		
	Vertical		9.77		24.09	25.36	29		34.07		46.45	49.58	53.94	58.88	
16.9	Cable		9.77		24.7	25.63		33.08	36.44				51.24		78.44
	Horizontal		9.77		24.67	25.65		33.09	36.44				51.06		
	Vertical		9.77			25.65	29.07	33.1	36.45		47.47				
18.2	Cable	5.74	9.77		24.87	26.15									80.2
	Horizontal	5.74	9.77		24.87	26.15	27.34	33.13	37.38				51.9	60.46	
	Vertical	5.74	9.77		24.87	26.15		33.14	37.4		48.97		51.99	60.44	
19.2	Cable		9.7	11.39	24.92	26.55	27.73		37.93				53.1	60.91	81.7
	Horizontal	5.49	9.7		24.91	26.56		33.04	37.92				52.53	60.76	
	Vertical		9.7	19.98	24.93	26.55	27.71	33	37.93			50	52.54	60.97	
20.2	Cable		9.7	11.54	24.95	26.99	29.95	33.02	38.51				53.96		85.63
	Horizontal	5.7	9.7		24.93	26.99	29.95	33.02	38.5				53.15		
	Vertical		9.7		24.96	26.99	29.97	33.02	38.5			51.06	53.21	61.46	
21.2	Cable		9.62	11.63	24.96	27.45	30.43	33	39.05				53.65	62.54	87
	Horizontal	5.76	9.63			27.45	30.43	33	39.07				53.7	62.4	
	Vertical	5.75	9.64	20.21	24.97	27.45	30.44	32.9	39.08				53.71	62.62	
21.9	Cable		9.61	11.7	24.97	27.68	30.71		39.36				53.35	62.92	87.75
	Horizontal	5.75	9.61			27.68		32.98	39.38				54.01		
	Vertical		9.61		24.99	27.68	30.72	32.98	39.36			52.69	54	62.74	
23	Cable		9.54	21.3		28.07	31.3	32.97	39.95				54.61	63.96	89.02
	Horizontal	5.74	9.54			28.08	31.3	32.96	39.96				54.6		
	Vertical		9.54	20.13	24.98	28.09	31.31	32.96	39.95				54.5		

Accordingly, the calculated cable force was 17.25 t, which was very similar to the strain gauge results (16.9 t).

Five sample test results are given in Fig. 17. Eqs. (3), (4) and (5) results were compared with the strain gauge results, from which the closest results were obtained with Eqs. (4) and (5).

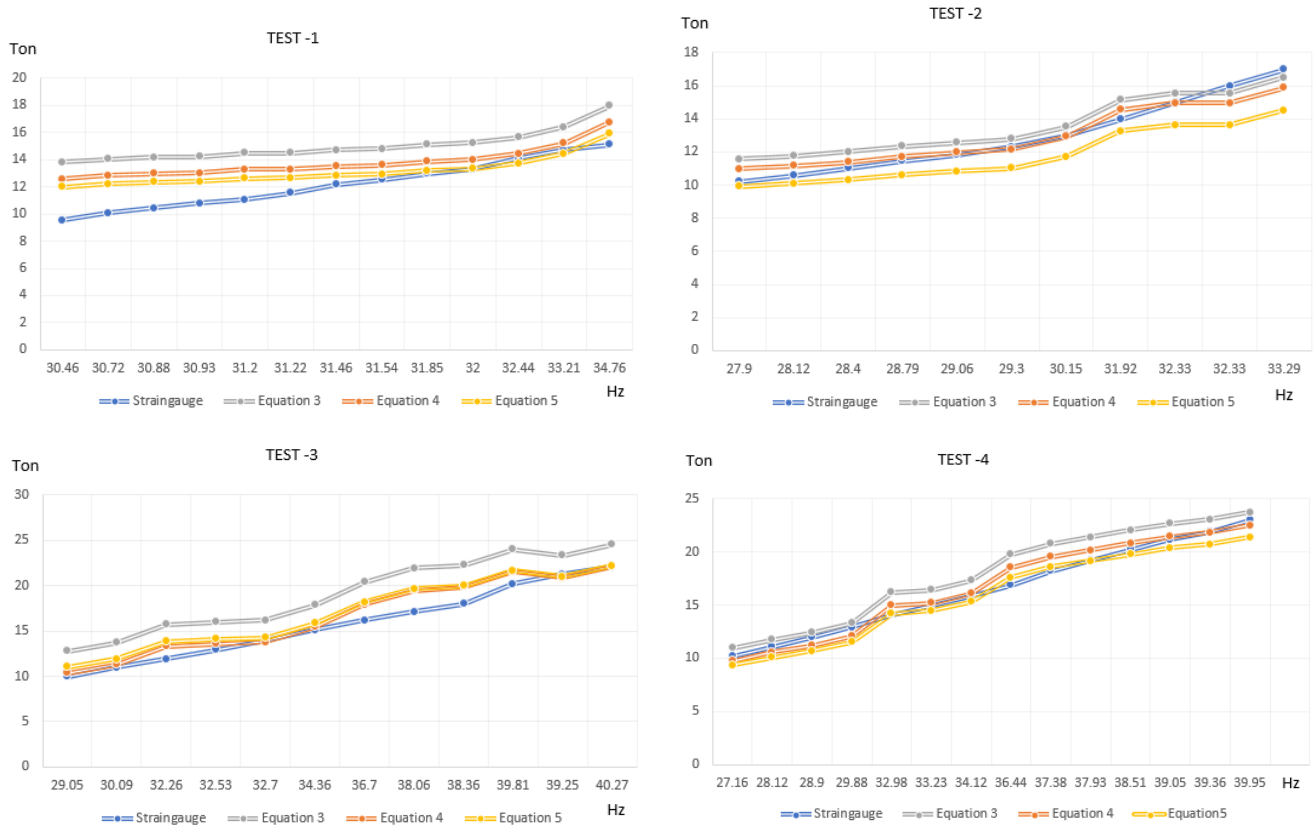

Fig. 17. Tests 1-4: cable forces - strain gauge results.

The equation results for the Test 1 start were quite different from the strain gauge results, which might have been because the accelerometer clamp was not fixed well to the cable. The other test results were in concert with the strain gauge results.

It was very difficult to see the second mode frequencies on the FFT graphics because they were very high and very close to the accelerometer progress up limits. The test second mode frequencies could be read more easily than the others could, and the closest results were found with Eq. 4, as can be seen in Fig. 18.

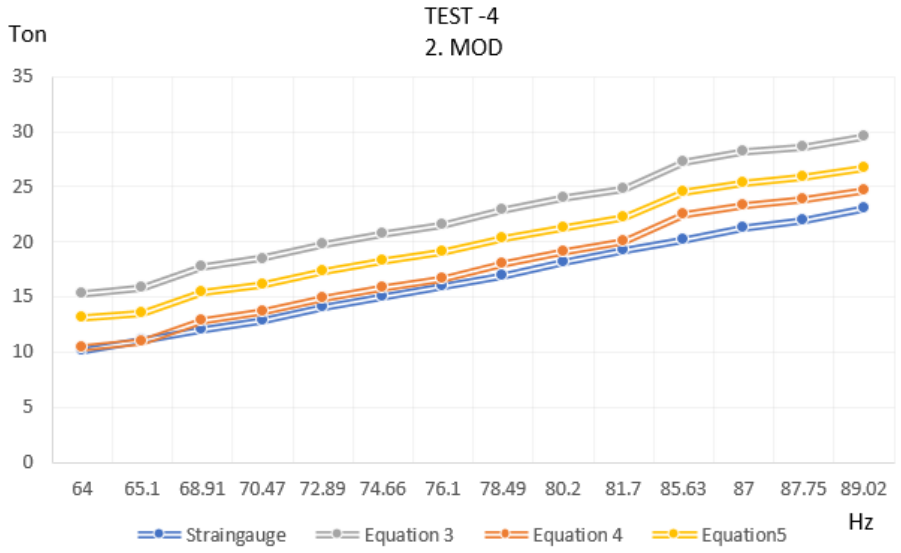

Fig. 18. Second mode: cable forces - strain gauge results.

The bearing capacity of the arch beam with a pre-tension cable was 15.5 t as opposed to 11.5 t without. Thus, as proposed in this study, it is obvious that when using arch beams with cables, the bearing capacity could be increased by 35%. All tests were finished whenever buckling of the beam flange occurred, as illustrated in Fig. 19.

Fig. 19. Buckling of a beam compression flange.

The buckling analysis was repeated for a single load during testing, the value of which was set at 7 t, to obtain the compression safety stress limit of the arch beam flange. Figs. 20 and 21 show the buckling mode characteristics for the conventional and arch beams, respectively.

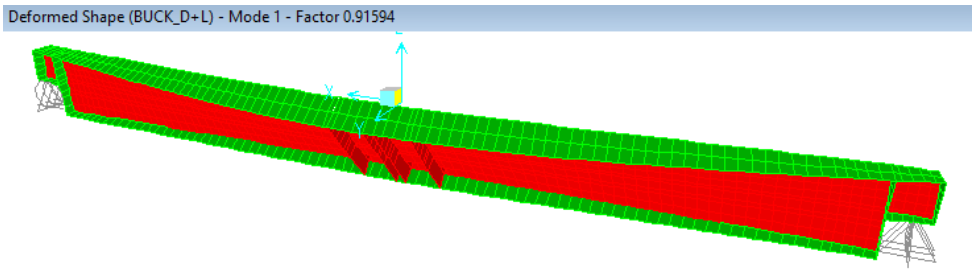

Fig. 20. Buckling mode of the conventional beam under a single load.

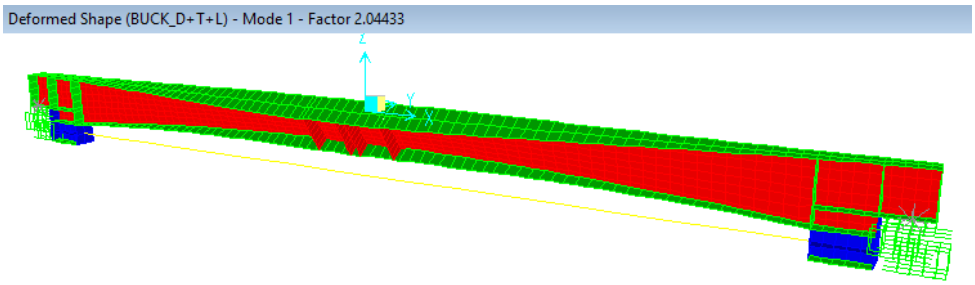

Fig. 21. Buckling mode of the pre-stressed arch beam under a single load.

Buckling mode factors were 0.91 and 2.04 for the conventional and arch beams, respectively. It is clear that 0.91 for the conventional beam was not sufficiently high as a safety factor and that 2.04 proves that the arch beam shape increased the bearing capacity of the beam considerably.

On the other hand, it might be possible to reduce flange stresses by increasing the cable tension force. Thus, it might be possible to obtain a higher load-bearing capacity for the beam proposed herein. The pre-tension force was increased up to 15 t and the finite element

analysis model of the beam was re-analyzed with the obtained stresses, as shown in Fig. 22.

In this case, the single load-bearing capacity was increased to 11.34 t (13.4%) and the pre-tension force was limited by the bottom flange compression safety stress. The 15 t pre-tension force generated 1.44 t/cm² compression stress at the bottom flange, which after the vertical loading, could be reduced by applying an additional pre-tension load to the cable. Thus, the system's maximum load bearing capacity could be increased much further with this method.

Temperature changes did not affect the system load or stress distribution by much at all. As an example, after applying a temperature increase of 5°C to the cable, the load change was only 230 kg and the stress difference was close to zero.

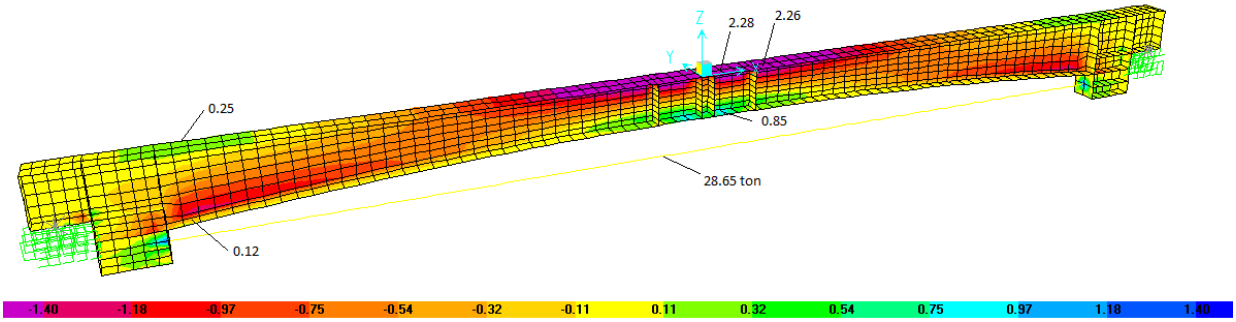

Fig. 22. Stress results for 15 t pre-tension force.

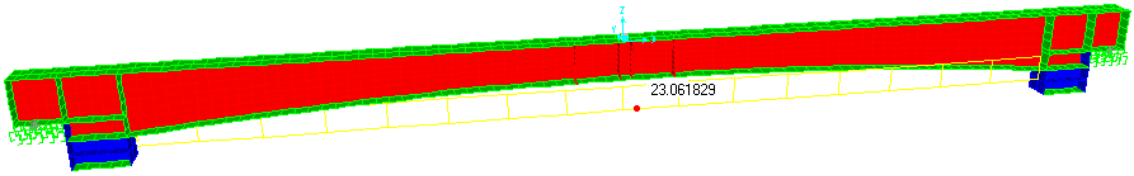

Fig. 23. The force on the cable before the temperature increase (load in tons).

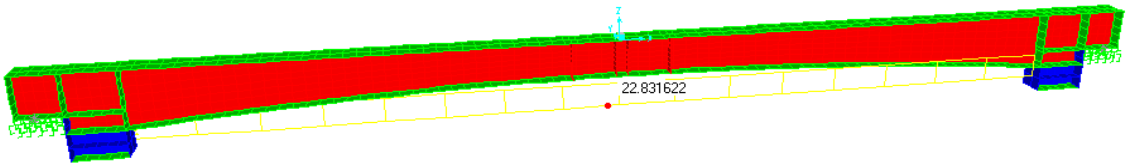

Fig. 24. The force on the cable after the 5°C temperature increase (load in tons).

The last beam test results with and without a cable are shown in Figs. 25 and 26, respectively. For the beam without a cable, only 4.18 t could be carried before reaching the safety stress level (beam failure without a cable is shown in Fig. 27). The load ratio was 7.11/4.18 =1.7, so the load bearing capacity with the cable increased by 70%.

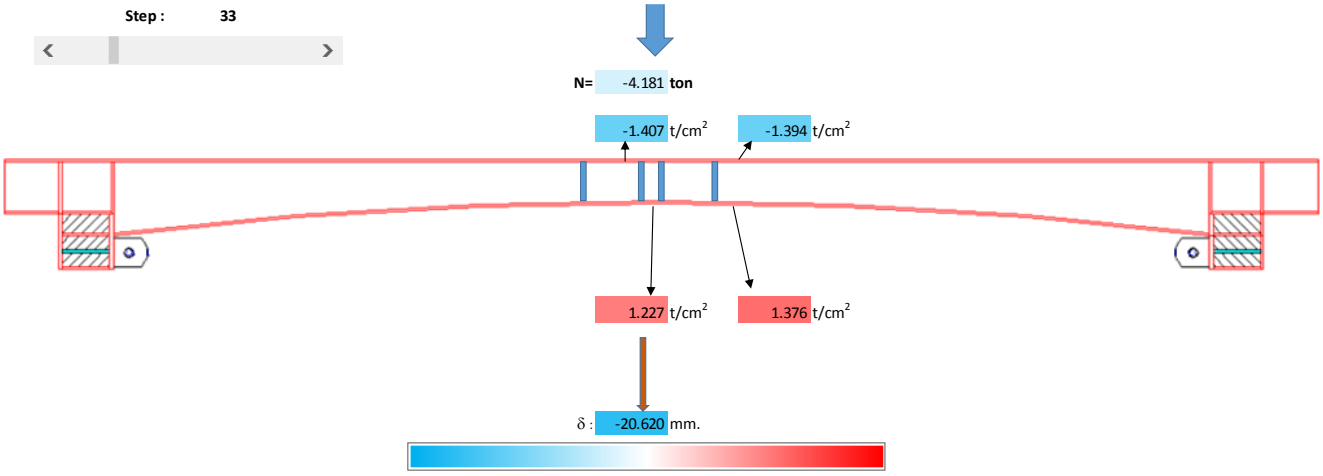

Fig. 25. Stress and displacement results for the arch beam without a cable.

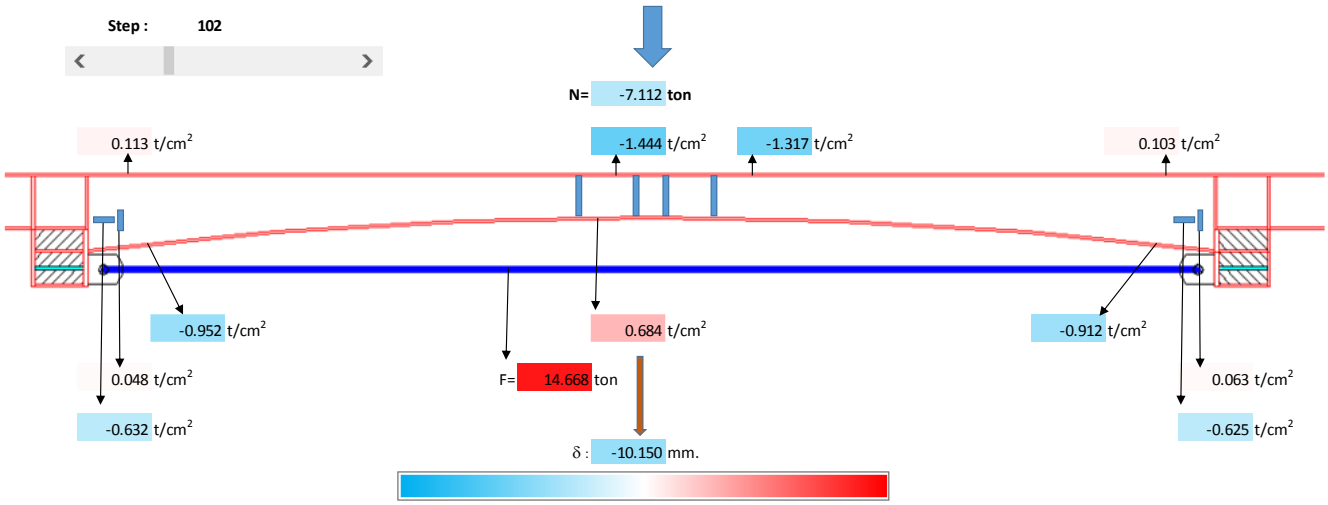

Fig. 26. Beam stress and displacement results for the arch beam with a cable.

Fig. 27. Test-5 beam (without a cable) after failure.

6. Conclusions

The load capacity of an arch beam supported by a pre-tension cable can be increased up to 2 times due to the fact that the compressive stress developed on the upper part of the beam is reduced by the adverse moment effect of the pretension force of the cable and decreasing the beam height at the mid-point of the span length causes an increase in the buckling load factor. There is no necessity for bracings to prevent lateral buckling of the top flange of the beam or for a reduction in beam height relative to the conventional hot-rolled beam section. This theory was proved by the buckling analysis. It was found that the bottom arch flange of the beam caused a delay in the buckling of the beam, which highlights a need to investigate new design methods to improve arch beam moment capacity.

The disadvantages of the proposed method are construction beam costs, cable pre-stressing, and stress losses that occur in the cable over time. However, the need for larger beams able to handle the same loads, the additional lateral joint elements required for beam stability, and the impact of these elements on the architectural appearance should actually balance or lower the overall costs. Moreover, the reduction of the pre-stressing force in the cable over time does not exceed 8% (Arda and Yardimci, 2000) and the temperature difference between the beam and cable should not be considered as a significant disadvantage.

The ease of passage of mechanical and electrical installations through the gap created by the belt shape of the beam which contemporarily gives a more architectural aesthetic appearance can be considered as a major advantage of arch beams supported by pre-tension cables, as proposed in this study. It is clear that when there is a sliding support structure, the simply supported system will not be affected by small temperature changes, and this ratio can be increased by adjusting the post-tension force on the cable if necessary.

REFERENCES

ANSI-AISC 360 (2010). Specification for Structural Steel Buildings. American Institute of Steel Construction (AISC), Chicago, USA.

Arda TS, Yardimci N (2000). Çelik Yapıda Öngerme. Birsen Yayınevi, İstanbul Turkey.

Humar JL (1990). Dynamics of Sstructures. Prentice Hall, New Jersey, USA.

IMO - 02/2008 (2008). Çelik Yapılar Hesap Kuralları ve Proje Esasları. Turkish Chamber of Civil Engineers (TMMOB/IMO), İstanbul, Turkey.

Wang ML, Chen ZL, Steve SK, George ML (2000). Magneto-elastic permeability measurement for stress monitoring in steel tendons and cables. *Proceedings of SPIE the International Society for Optical Engineering*, Vol. 3995, 492-500.

Zhi F, Jian-qun W (2012). Practical formula for cable tension estimation by vibration method. *Journal of Bridge Engineering*, 17(1), 161-164.